Unsupervised and Accurate Extraction of Primitive Unit Cells from Crystal Images

Niklas Mevenkamp, Benjamin Berkels

AICES Graduate School
RWTH Aachen University, Germany
mevenkamp@aices.rwth-aachen.de, berkels@aices.rwth-aachen.de

Abstract. We present a novel method for the unsupervised estimation of a primitive unit cell, i.e. a unit cell that can't be further simplified, from a crystal image. Significant peaks of the projective standard deviations of the image serve as candidate lattice vector angles. Corresponding fundamental periods are determined by clustering local minima of a periodicity energy. Robust unsupervised selection of the number of clusters is obtained from the likelihoods of multi-variance cluster models induced by the Akaike information criterion. Initial estimates for lattice angles and periods obtained in this manner are refined jointly using non-linear optimization. Results on both synthetic and experimental images show that the method is able to estimate complex primitive unit cells with sub-pixel accuracy, despite high levels of noise.

1 Introduction

The analysis and classification of the symmetry of crystalline structures is a fundamental necessity in various scientific fields, such as biology, chemistry and materials science [7,12,13,20]. Experimental analyses are often based on diffraction patterns, e.g. from X-rays [15] or electrons [21]. The most common technique for symmetry extraction from crystalline images is the classification of the Bragg reflections [3], i.e. relating the positions of image peaks in Fourier space with the lattice vectors of the crystal. This direct relation is the foundation for a variety of image processing techniques aimed at analyzing crystals or removing artifacts from corresponding images [14].

Recently, real-space methods have proven to be very powerful for a wide range of processing tasks on crystal images, such as grain segmentation [2], crystal defect localization [10], noise reduction [16] and sample drift correction [19]. All of these methods have in common that they exploit the (average) crystal symmetry in some way or another. Thus, they require prior knowledge on the geometry of the corresponding (perfect) crystals. Typically, the necessary crystal lattice parameters are estimated either manually or using Fourier-based techniques, which often also requires manual assessment in order to correct errors due to image distortion, noise and ambiguities. Thus, an entirely unsupervised use of these otherwise automated processing methods is usually not possible.

In [19], Sang and LeBeau proposed a new real-space method for lattice angle estimation based on *projective standard deviations* (PSD). While the method outperforms Fourier methods in accuracy and robustness to noise, it still needs manual input to relate PSD peaks with the corresponding lattice directions.

The goal of this paper is to overcome the necessity for manual input in crystal lattice extraction from images. To this end, we propose a novel unsupervised real-space method to estimate primitive unit cells from crystal images. In particular, we show how fundamental periods can be estimated robustly from 1D signals.

2 Methods

A crystal can be characterized by the positions and types of its elements, i.e. $\mathscr{C} \subset \mathbb{R}^d \times \mathbb{R}$. In case $d = 3$, the elements are typically atoms and their type is given by the atomic number. An important property of crystals is their symmetry. It allows for a decomposition of $\mathscr{C}$ into a *unit cell* $U = \{\boldsymbol{v}_1, \dots, \boldsymbol{v}_d\} \subset \mathbb{R}^d$, which defines the repeating pattern of the crystal, and the corresponding *motif* $M = M_{\mathscr{C}}(U) = \{(\boldsymbol{m}_1, c_1), \dots, (\boldsymbol{m}_{n_U}, c_{n_U})\} \subset \mathbb{R}^d \times \mathbb{R}$, which defines the relative positions and types of the $n_U \in \mathbb{N}$ elements within the unit cell U. This results in the following representation of the crystal:

$$\mathscr{C}(U, M) = \left\{ \left(\boldsymbol{m}_j + \textstyle\sum_{i=1}^{d} z_i \boldsymbol{v}_i, c_j \right) \,\middle|\, z_i \in \mathbb{Z} \text{ for } 1 \le i \le d,\ 1 \le j \le n_U \right\} . \quad (1)$$

Note that this decomposition is not unique. For any given crystal $\mathscr{C}$,

$$\mathcal{U}_{\mathscr{C}} = \{U \subset \mathbb{R}^d \,|\, \#(U) = d \wedge \exists M \subset \mathbb{R}^d \times \mathbb{R} : \#(M) < \infty \wedge \mathscr{C}(U, M) = \mathscr{C}\} \quad (2)$$

denotes the set of all of its unit cells. Then

$$\mathcal{U}^p_{\mathscr{C}} = \{U \in \mathcal{U} \,|\, \#(M_{\mathscr{C}}(U)) = \min_{U' \in \mathcal{U}_{\mathscr{C}}} \#(M_{\mathscr{C}}(U'))\} \quad (3)$$

is the set of *primitive* unit cells. The Bravais lattice

$$V_{\mathscr{C}} = \left\{ \textstyle\sum_{i=1}^{d} z_i \boldsymbol{v}_i \,\middle|\, \{\boldsymbol{v}_1, \dots, \boldsymbol{v}_d\} \in \mathcal{U}^p_{\mathscr{C}}, z_1, \dots, z_d \in \mathbb{Z} \right\} \quad (4)$$

is called *crystal lattice*, i.e. its elements are lattice points. Since $0 \in V_{\mathscr{C}}$, any $v \in V_{\mathscr{C}}$ can be interpreted as a vector connecting two lattice points. Such a vector is called *lattice vector*. For an introduction to this terminology from a mineral science point of view, we refer to [18]; for an illustration see Figure 1.

$\mathcal{U}_{\mathscr{C}}$ can also be characterized by

$$\mathcal{U}_{\mathscr{C}} = \{\{\boldsymbol{v}_1, \dots, \boldsymbol{v}_d\} \subset V_{\mathscr{C}} \,|\, \boldsymbol{v}_1, \dots, \boldsymbol{v}_d \text{ linear independent } \} . \quad (5)$$

Furthermore, $\{\boldsymbol{v}_1, \dots, \boldsymbol{v}_d\} \in \mathcal{U}_{\mathscr{C}}$ is primitive if and only if the parallelepiped (or a parallelogram in two dimensions) spanned by $\boldsymbol{v}_1, \dots, \boldsymbol{v}_d$ contains no lattice point $\boldsymbol{v} \in V_{\mathscr{C}}$ other than its corner points.

In this paper, we discuss how to extract a primitive unit cell from a two-dimensional experimental image of a projected crystal. The original crystal is

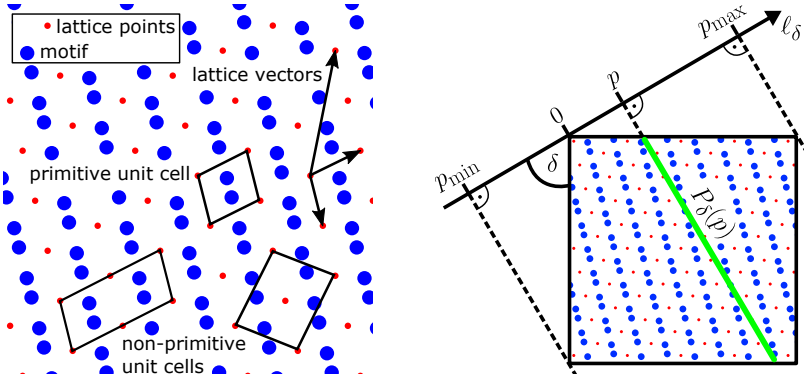

Fig. 1. Left: crystal lattice (red dots) with a minimal motif of size two (pairs of blue dots); Right: illustration of the points $P_\delta(p)$ in the image projected onto the line ℓ_p

three dimensional and during acquisition its orientation is manually refined until the desired projection - orthogonal to one of its unit cell vectors - is retrieved. This results in a crystal $\mathscr{C} \subset \mathbb{R}^2 \times \mathbb{R}$. In the following, we assume that the projection and the modality of the crystal image retain a unique identification of the elements in the crystal $\mathscr{C}$ and a unique relation to the image intensities.

Then, in an ideal setting, such an image $f : \Omega = (0,1)^2 \to \mathbb{R}$ fulfills

$$f(x + z_1\boldsymbol{v}_1 + z_2\boldsymbol{v}_2) = f(x)\ \forall x \in \Omega\, \forall z_1, z_2 \in \mathbb{Z} : x + z_1\boldsymbol{v}_1 + z_2\boldsymbol{v}_2 \in \Omega \tag{6}$$

for any two lattice vectors $\boldsymbol{v}_1, \boldsymbol{v}_2 \in V_{\mathscr{C}}$. Thus, lattice vectors are minimizers (in the ideal setting also roots) of the following energy:

$$E(\boldsymbol{v}_1, \boldsymbol{v}_2) = \sum_{(z_1,z_2)\in\mathcal{Z}} \int_{x\in\tilde{\Omega}} \left(f(x) - f(x + z_1\boldsymbol{v}_1 + z_2\boldsymbol{v}_2)\right)^2 \,\mathrm{d}x\,, \tag{7}$$

where $\mathcal{Z} = \{(1,0),(0,1),(1,1)\}$ and $\tilde{\Omega} \subset \Omega$ has to be chosen in a suitable way for the desired lattice vectors, which will be addressed later. In other words, $\boldsymbol{v}_1, \boldsymbol{v}_2 \in V_{\mathscr{C}} \Leftrightarrow E(\boldsymbol{v}_1, \boldsymbol{v}_2) = 0$. Moreover, the following non-parallel lattice vectors

$$(\boldsymbol{v}_1, \boldsymbol{v}_2) \in \underset{(\boldsymbol{u}_1,\boldsymbol{u}_2)\in\{E=0\}\cap\{\boldsymbol{u}_1\times\boldsymbol{u}_2\neq 0\}}{\arg\min} |\boldsymbol{u}_1| + |\boldsymbol{u}_2| \tag{8}$$

form a primitive unit cell, since the parallelogram spanned by two shortest lattice vectors cannot contain any lattice points other than its corner points.

While obtaining a primitive unit cell may seem trivial at this point, it turns out to be very challenging in practice without manual input. Noise, image distortions and crystal defects result in the energy E being non-zero except for $\boldsymbol{v}_1, \boldsymbol{v}_2 = 0$ or $|\boldsymbol{v}_1|, |\boldsymbol{v}_2| > \mathrm{diam}\Omega$. Nevertheless, due to the regularity imposed by the integration, $\{\boldsymbol{v}_1, \boldsymbol{v}_2\} \in \mathcal{U}_{\mathscr{C}}$ still implies $\nabla E(\boldsymbol{v}_1, \boldsymbol{v}_2) = 0$. However, the reverse implication is not true in general. Figure 2 illustrates one potential pitfall. There are two types of local minima. The one with larger energy corresponds to the

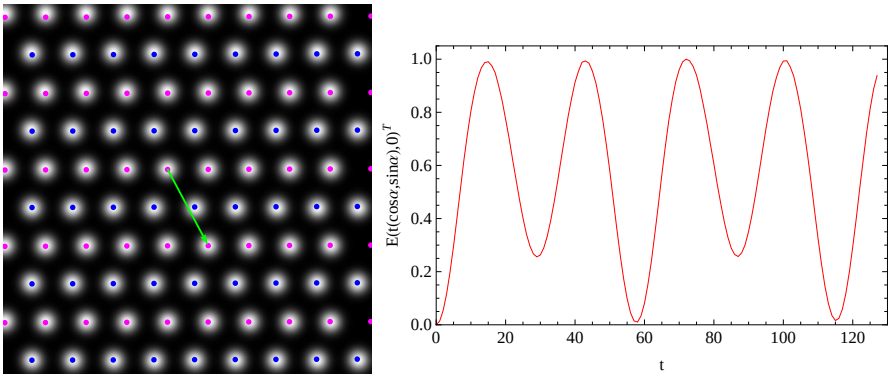

Fig. 2. Left: artificial crystal lattice (magenta dots) with a motif of size two (a magenta/blue dot pair is a motif copy). Right: normalized energy (7) for $\boldsymbol{v}_1 = t(\cos\alpha, \sin\alpha)^T, \boldsymbol{v}_2 = 0$ as a function of t with $\alpha = -61.95°$ (green vector)

spacing between diagonally neighboring atoms, but the actual lattice points skip one row and belong to twice the spacing, i.e. the minima with smaller energy.

Furthermore, $\nabla E(\boldsymbol{v}_1, \boldsymbol{v}_2) = 0$ implies $\nabla E(n_1\boldsymbol{v}_1, n_2\boldsymbol{v}_2) = 0$ for all $n_1, n_2 \in \mathbb{Z}$. Thus, it is likely that minimization of E converges to a local minimum that either does not correspond to a unit cell at all, or not to a primitive one.

In the following, we will discuss a method that allows for an efficient estimation of primitive lattice vectors from E based on a sophisticated strategy for finding the desired local minima. The strategy is split into three parts: approximation of 1) *lattice vector angles* and 2) *fundamental periods*, and 3) refinement of the resulting approximate primitive unit cell.

2.1 Real-space Analysis of Lattice Vector Angles

Any $\alpha \in [0, 2\pi]$ such that there is a $t \in (0, \infty)$ with $t\boldsymbol{e}_\alpha = t(\cos\alpha, \sin\alpha)^T \in V_{\mathscr{C}}$ is called *lattice vector angle*. In the following, we briefly recall a recent real-space method to estimate lattice vector angles by Sang and LeBeau [19]. Let $\pi_\delta(x) = (x_1 \cos\delta + x_2 \sin\delta)\,\boldsymbol{e}_\delta$ be the projection of a point $x \in \Omega$ onto the line $\ell_\delta(p) = p\boldsymbol{e}_\delta$ and $P_\delta(p) = \pi_\delta^{-1}(p)$ the points in Ω that are projected onto $\ell_\delta(p)$ (see Figure 1). Then, the average intensity of the image projected onto $\ell_\delta(p)$ is

$$A_\delta(p) = \fint_{P_\delta(p)} f \,\mathrm{d}x \text{ for } |P_\delta(p)| > 0 \text{ and zero else .} \tag{9}$$

Here, for $B \subset \mathbb{R}^d$, $\fint_B f\,\mathrm{d}x = \frac{1}{|B|}\int_B f\,\mathrm{d}x$ is the integral mean. Let $x_1^c = (0,0)^T$, $x_2^c = (0,0)^T$, $x_3^c = (1,0)^T$, $x_4^c = (1,1)^T$ denote the corners of $\Omega = (0,1)^2$ and $p_{\min} = \min_{i=1,\dots,4} \pi(x_i^c)$, $p_{\max} = \max_{i=1,\dots,4} \pi(x_i^c)$ the lower and upper bounds of their projections onto ℓ_δ. Then, using the interval $[p_{\min}, p_{\max}]$ as a bound for

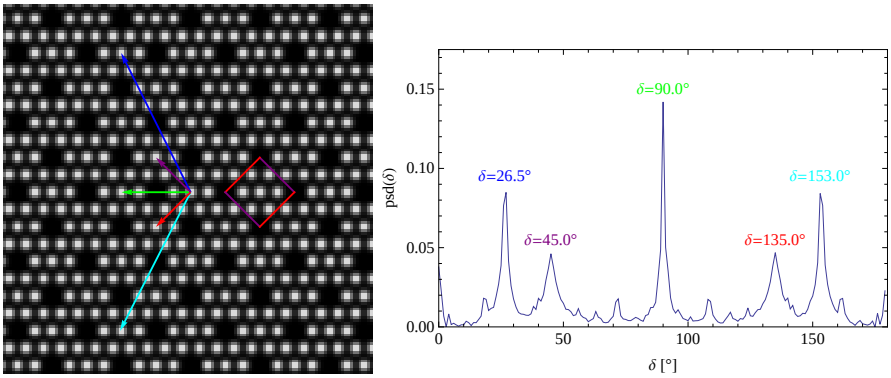

Fig. 3. Left: hex lattice with vacancies, vectors $T_{\alpha_i}\boldsymbol{e}_{\alpha_i}$, $i = 1, \dots, 5$ (blue, purple, green, red, cyan), primitive unit cell (purple/red box); Right: psd for $\delta \in [0, \pi]$

the support of A_δ, we define the *projective standard deviation* as (cf. [19])

$$\mathrm{psd}(\delta) = \sqrt{\fint_{p_{\min}}^{p_{\max}} \left(A_\delta(p) - \mu_\delta\right)^2 \,\mathrm{d}p}, \;\; \mu_\delta = \fint_{p_{\min}}^{p_{\max}} A_\delta(p)\,\mathrm{d}p\,. \tag{10}$$

Significant peaks $(\delta_1, \dots, \delta_n)$ of the signal $\mathrm{psd} : [0, 2\pi] \to \mathbb{R}_{\geq 0}$ are indicators that the image f is periodic along the perpendicular directions, i.e. $\alpha_i = \delta_i + \frac{\pi}{2}$, $i = 1, \dots, n$ are lattice vector angles: As in the 3D case, projecting a 2D crystal along any of its lattice vectors, i.e. onto a line perpendicular to the lattice vector, yields a periodic signal, which is of high standard deviation.

Let us point out that the psd alone does not suffice to select two lattice vector angles. Consider the example shown in Figure 3. Selecting the two highest peaks yields the lattice vector angles $\alpha_1 = 180°$ (green vector) and $\alpha_2 = 116.5°$ (blue vector) or $\alpha_2 = 243°$ (cyan vector). Lattice vectors pointing in these directions cannot form a primitive unit cell. Possible pairs resulting in primitive unit cells in this case are the blue & purple, purple & green, green & red, red & cyan and purple & red vectors, while only the latter results in a primitive unit cell satisfying (8). Since Sang and LeBeau [19] do not address this issue, we propose to select a suitable pair of lattice vector angles in an unsupervised fashion by finding one that satisfies (8). However, this requires knowledge of the corresponding fundamental periods.

2.2 Real-space Analysis of Fundamental Periods

For any lattice vector angle α, let $\mathcal{T}_\alpha = \{t \in (0, \infty) \,|\, t\boldsymbol{e}_\alpha \in V_{\mathscr{C}}\}$. Then, the *fundamental period* is $T_\alpha = \min \mathcal{T}_\alpha$. In the following, we props a method to estimate T_α from an image f of the corresponding crystal $\mathscr{C}$.

We consider the one-dimensional energy

$$E_\alpha(t) = \fint_{\Omega_\alpha(t)} \left(f(x + t\boldsymbol{e}_\alpha) - f(x)\right)^2 \,\mathrm{d}x\,, \tag{11}$$

where $\Omega_\alpha(t) = \{x \in \Omega \,|\, x + t\boldsymbol{e}_\alpha \in \Omega\}$. Assuming that f is exactly periodic along the direction $\boldsymbol{e}_\alpha$ yields $\mathcal{T}_\alpha = E_\alpha^{-1}(0) \setminus \{0\}$. Thus, in an ideal situation, we have $T_\alpha = \min(E_\alpha^{-1}(0) \setminus \{0\})$. In practice, however, distortions and noise in the image f, as well as errors in the angle α prohibit such a classification of the fundamental period. Still, elements of $\mathcal{T}_\alpha$ should be local minimizers of E_α. Let

$$S_\alpha = \{t \in (0,\infty) \,|\, \exists \delta > 0 \; \forall s \in [t-\delta, t+\delta] \setminus \{t\} : E_\alpha(t) < E_\alpha(s)\} \tag{12}$$

denote the set of isolated local minima of E_α except for $t = 0$. Unfortunately, as illustrated in Figure 2, possibly $(\min S_\alpha)\boldsymbol{e}_\alpha \notin V_{\mathscr{G}}$. Thus, we need a robust way to select the desired local minimum from S_α.

Let us assume that all errors (image noise, distortions, discretization) are small enough that the energy E_α at least fulfills the following properties:

I The (numerical) fundamental period of the signal E_α is close to T_α
II Multiples of T_α lie near local minimizers of E_α
III The local minimizer with smallest energy is roughly a multiple of T_α
IV Distances between energies of local minimizers close to multiples of T_α are smaller than those between them and the energies of other local minimizers

Note that in an ideal setting, these properties are a consequence of (6).

Property I implies that $E_\alpha(S_\alpha)$ may be split in $k \leq \#(\{t \in S_\alpha \,|\, t \leq T_\alpha\})$ clusters $C_1, \ldots, C_k$ corresponding to the different types of local minima in each fundamental period of E_α. Moreover, due to Properties II-IV, the cluster containing $\min E_\alpha(S_\alpha)$ also contains $E_\alpha(T_\alpha)$, but no $E_\alpha(t)$ with $t \notin \mathcal{T}_\alpha$. Thus, T_α can be estimated as $\hat{T}_\alpha = \min(E^{-1}(C_i) \cap S_\alpha)$, where $1 \leq i \leq k$ with $\min E_\alpha(S_\alpha) \in C_i$.

The proper choice of the number of clusters is crucial in this context: on the one hand, if k is chosen too small, one risks that a local minimum corresponding to a period $t < T_\alpha$ ends up in the same cluster as $E(T_\alpha)$, which implies $\hat{T}_\alpha \neq T_\alpha$; on the other hand, if k is chosen too large, one risks that $E_\alpha(T_\alpha)$ does not end up in the same cluster as $\min E_\alpha(S_\alpha)$, also resulting in $\hat{T}_\alpha \neq T_\alpha$.

To this end, we propose a method for robust unsupervised selection of the number of clusters k. Our approach is based on work by Pelleg and Moore [17]. They use a Bayesian information criterion (BIC) under an identical spherical Gaussian assumption on the cluster formation to formulate an unsupervised variant of k-means, known as X-means. Note that G-means [11], which has been shown to outperform X-means, especially in higher dimensions, is not suitable for our setting, because the total number of data points $\#(S_\alpha)$ is very small.

We base our analysis on the Akaike information criterion $AIC_k = -2\hat{L}_k + 2p_k$ [1], where $\hat{L}_k = \hat{L}_k(S) = \max_\theta L_k(S|M_k(\theta))$ is the maximum of the log-likelihood

$$L_k(S|M_k(\theta)) = \log \prod_{j=1}^n P(x_j|M_k(\theta)) = \sum_{j=1}^n \log P(x_j|M_k(\theta)) \tag{13}$$

of the data $S = \{x_1, \ldots, x_n\}$ given a model $M_k(\theta)$ of the data, which induces point probabilities $P(x_j|M_k(\theta))$. As pointed out in [6], AIC has theoretical and practical advantages over BIC. For instance, it allows for the evaluation of actual model likelihoods, allowing for more sophisticated strategies to select a proper k than simply minimizing the value of the criterion, as is usually done with BIC.

In our setting, let $M_k(\theta)$ model the set $S_\alpha = \{x_1, \ldots, x_n\}$ as k one-dimensional Gaussian distributions with means $\mu_1, \ldots, \mu_k$, $\mu_i \neq \mu_l$, $i \neq l$, variances $\sigma_1^2, \ldots, \sigma_k^2$, and relative frequencies $\frac{n_1}{n}, \ldots, \frac{n_k}{n}$. Then

$$P(x_j|M_k(\theta)) = \frac{n_{(j)}}{n}\left(2\pi\sigma_{(j)}^2\right)^{-1/2} \exp\left\{-|x_j - \mu_{(j)}|^2/(2\sigma_{(j)}^2)\right\} . \tag{14}$$

Here, $(j) = \min\{i \in \{1, \ldots, k\} \,|\, |x_j - \mu_i|^2 \leq |x_j - \mu_l|^2 \,\forall l \neq i\}$. Usually, there is only one such i. Since $n_k = n - \sum_{i=1}^{k-1} n_i$, the set of free model parameters is $\theta = (n_1, \ldots, n_{k-1},\, \mu_1, \ldots, \mu_k,\, \sigma_1, \ldots, \sigma_k)$. The maximum-likelihood estimator $\hat{\mu}_i = \frac{1}{n_i}\sum_{x \in C_i} x$ is obtained as a result from the k-means clustering for each cluster C_i. The maximum-likelihood estimator of the variance is $\hat{\sigma}_i^2 = \frac{1}{n_i}\sum_{x \in C_i}(x - \hat{\mu}_i)^2$. This leads to the following expression for the maximum log-likelihood of S:

$$\hat{L}_k(S) = \sum_{i=1}^{k}\left[n_i \log\tfrac{n_i}{n} - \tfrac{1}{2}n_i\left(\log\left(2\pi\hat{\sigma}_i^2\right) + 1\right)\right] . \tag{15}$$

In this setting, the number of free parameters is $p_k = 3k - 1$.

As pointed out by Akaike, the likelihood of the model M_k given the data S is $\mathcal{L}(M_k|S) = \exp\{(AIC_{k_{\min}} - AIC_k)/2\}$, where $k_{\min} = \arg\min_k AIC_k$. Note that $\mathcal{L}(M_{k_{\min}}|S) = 1$. Models with a likelihood not significantly less than 1 cannot be discarded with confidence. In case two or more models cannot be discarded, we suggest to prefer models assuming fewer clusters in order to increase the probability that the desired local minimum $E_\alpha(T_\alpha)$ is assigned to the same cluster as the global minimum $\min E_\alpha(S_\alpha)$. Thus we suggest to choose the optimal number of clusters as

$$k^* = \min\{k \,|\, \mathcal{L}(M_k|S) > \tau\} . \tag{16}$$

We used the threshold $\tau = 0.1$ for all presented experiments and found that in the regarded cases the result was not sensitive to this particular choice.

Using the unsupervised k-means clustering described above, we can assign a fundamental period T_α to any given lattice vector angle α. Let $\alpha_1, \ldots, \alpha_n$ be candidate lattice vector angles estimated as described in Section 2.1 and $V^* = \{T_{\alpha_1}\boldsymbol{e}_{\alpha_1}, \ldots, T_{\alpha_n}\boldsymbol{e}_{\alpha_n}\} \subset V_{\mathscr{C}}$. Finally, in accordance with (8), we estimate the primitive unit cell by

$$U = \{\boldsymbol{v}_1, \boldsymbol{v}_2\}, \quad \boldsymbol{v}_1 = \operatorname*{arg\,min}_{\boldsymbol{u} \in V^*} \tfrac{1}{2}|\boldsymbol{u}|^2, \quad \boldsymbol{v}_2 = \operatorname*{arg\,min}_{\boldsymbol{u} \in V^* \setminus \{\boldsymbol{v}_1\}} \tfrac{1}{2}|\boldsymbol{u}|^2 . \tag{17}$$

2.3 Local Refinement of Lattice Vectors

The methods described above yield a good approximation of a primitive unit cell $U = \{\boldsymbol{v}_1, \boldsymbol{v}_2\} \in \mathcal{U}_{\mathscr{C}}^p$. However, by first estimating the angles of the desired lattice vectors followed by an estimation of their magnitudes, errors in the angles α_1, α_2 amplify the error in the magnitudes $|\boldsymbol{v}_1|, |\boldsymbol{v}_2|$. Nevertheless, the initial guess $\boldsymbol{v}_1, \boldsymbol{v}_2$ is expected to yield local convergence of iterative minimization of (7) to the desired local minimum. This minimization can be performed efficiently in practice, since the discretization of (7) is a sum of squares, which allows for

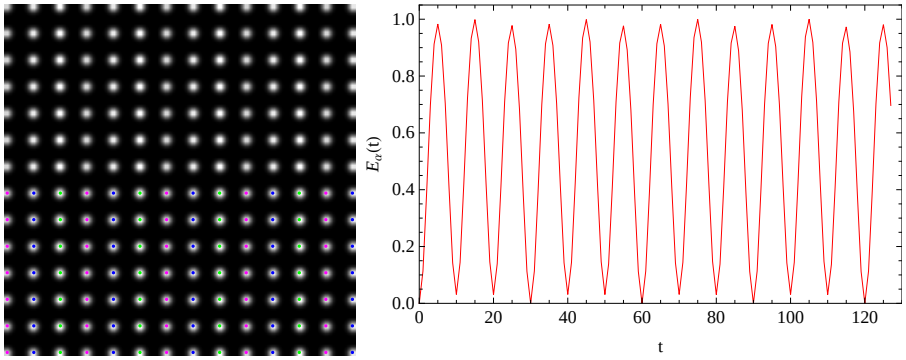

Fig. 4. Left: rectangular crystal lattice (magenta dots) with a motif of three very similar Gaussian bells placed along the horizontal lattice direction (magenta/blue/green dot triples); Right: $E_\alpha(t)$ (11) for $\alpha = 0$, i.e. the horizontal lattice direction

Gauss-Newton type algorithms to be used for numerical minimization. Finally, $\tilde{\Omega} = \{x \in \Omega \,|\, \mathrm{dist}(x, \partial\Omega) > \max\{|\boldsymbol{v}_1|, |\boldsymbol{v}_2|, |\boldsymbol{v}_1 + \boldsymbol{v}_2|\} + \epsilon\}$ can be used as the admissible set, with a fairly small ϵ (e.g. three times the pixels size), since the solution is not expected to be more than a few pixels away from the initial guess.

3 Results and Discussion

Here, we show unsupervised analyses of exemplary crystal structures, using both artificially created images, as well as electron micrographs acquired by scanning transmission electron microscopy (STEM) [4]. In the following figures, the *origin* of any crystal lattice is aligned manually with one of the atoms in the unit cell. Also, motif recognition is not part of the proposed method and was done manually to illustrate the full geometry of the crystals. The lattice and the motive is only overlayed in the lower half of each image to facilitate a visual confirmation of the correctness of the estimated lattice parameters.

Figure 4 shows an artificial rectangular crystal lattice with three 2D Gaussian bells of similar intensity in each primitive unit cell, placed along the horizontal lattice direction. The proposed estimator for the number of clusters yields the correct result ($k = 3$) for E_α with $\alpha = 0$, even though the absolute values of the local minima are extremely close to each other.

The accuracy of the proposed method is assessed on four artificially created crystal lattices (cf. Figure 5) with known parameters and varying levels of Gaussian noise. The resulting absolute errors in Table 1 show sub-pixel accuracy in all cases except for the "Bumps3" image in Figure 5 with 50% noise standard deviation. In this case, the combination of strong noise and low contrast between local minima constitutes a violation of Property IV, resulting in a third of the period to be estimated - hence the large error. Note that a classical Fourier analysis, e.g. selecting the two brightest non-collinear peaks in Fourier space, does not yield useful results for the images shown in Figure 5.

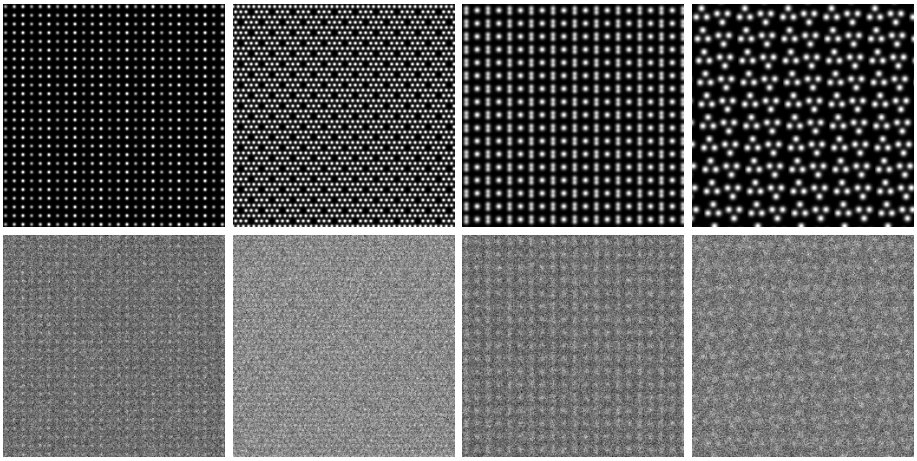

Fig. 5. Artificial crystal lattice images; top row: ideal crystals (from left to right: "Bumps3", "HexVacancy", "SingleDouble", "Triples2"); bottom row: same images plus Gaussian noise with a standard deviation of 50% of the maximum intensity

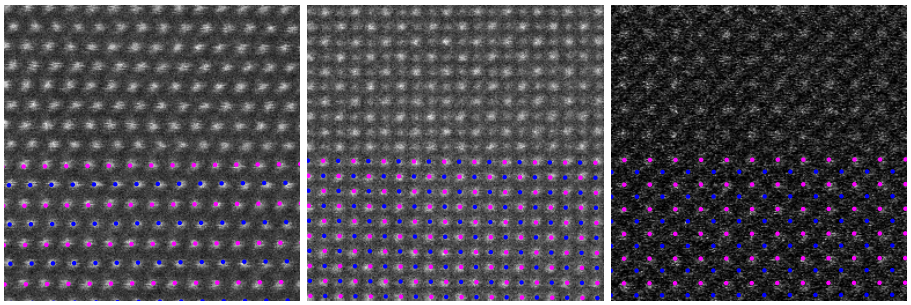

Fig. 6. Experimentally acquired STEM images and estimated crystal lattices (magenta dots) and motifs (magenta/blue dot pairs); STEM images courtesy of P. M. Voyles

Figure 6 shows experimental crystal images acquired using STEM. These images exhibit all artifacts inherent to this particular acquisition technique, namely intensity noise, small scale distortions and large scale sample drift. In the left image, along the roughly diagonal ($\alpha \approx -60°$) and vertical lattice directions, there is a horizontal offset between neighboring atoms (slight in the former and more apparent in the latter case). The proposed estimator (17) correctly identifies this and chooses the horizontal and vertical lattice vectors - the latter with a period that skips each second row of atoms (leaving the atoms in the other rows as part of the motif). In the right image, a similar difficulty is tackled, where a translation along the diagonal direction leads to high-auto correlation.

In [16], we recently proposed a method to denoise crystal images by non-local averaging over periodic lattices. This method showed a substantial performance increase over non-local averaging techniques [5,8] without such prior information.

Table 1. Errors in the lattice vectors detected by our method for the images from Figure 5. $\sigma / \max f$ is the noise standard deviation relative to the maximal image intensity

Crystal	$\sigma / \max f$	$\lvert \boldsymbol{v}_1^* - \boldsymbol{v}_1 \rvert$	$\lvert \boldsymbol{v}_2^* - \boldsymbol{v}_2 \rvert$
Bumps3	0	2.60×10^{-8}	4.13×10^{-8}
Bumps3	10%	0.136	0.0670
Bumps3	50%	0.425	22.3
HexVacancy	0	3.61×10^{-8}	1.50×10^{-7}
HexVacancy	10%	0.218	0.408
HexVacancy	50%	0.292	0.153
SingleDouble	0	2.20×10^{-10}	1.30×10^{-9}
SingleDouble	10%	0.0937	0.0830
SingleDouble	50%	0.360	0.306
Triples2	0	2.12×10^{-9}	8.84×10^{-9}
Triples2	10%	0.0129	0.0240
Triples2	50%	0.0172	0.009 00

However, the accuracy of our previously proposed approach to unsupervised lattice vector estimation is limited due to its Fourier space lattice angle estimation and likely unable to cope with complex motifs due to the employed period estimation via real-space sine fitting. Experiments performed for a selection of images from [16] indicate that the peak signal-to-noise ratio (PSNR) of the denoised image can be increased by more than 1 dB just by using the proposed real-space lattice vector estimation within the non-local denoising framework.

4 Conclusions

We have proposed a method for the unsupervised extraction of primitive unit cells from crystal images. It involves the selection of desired local minima of a periodicity energy by means of unsupervised clustering. Building on X-means [17], an improved strategy for the unsupervised selection of the number of clusters was proposed, using an extended data model considering clusters of different variances, and based on true model likelihoods derived from AIC.

Results on synthetic and experimental images demonstrate that the clustering robustly selects the desired local minimum and that primitive unit cells are estimated with sub-pixel accuracy, even in the presence of strong noise and ambiguities due to strong auto-correlation of the image along lattice vectors and inside the unit cells.

The proposed method offers the potential to turn powerful real-space processing methods for crystal images requiring prior knowledge about crystal symmetries into unsupervised methods. Lastly, let us point out that the proposed estimator for the fundamental frequency also suggests itself for pitch detection problems in sound analysis [9,22].

Acknowledgments The authors would like to thank P. M. Voyles for providing experimental STEM images.

References

1. Akaike, H.: A new look at the statistical model identification. Automatic Control, IEEE Transactions on 19(6), 716–723 (1974)
2. Boerdgen, M., Berkels, B., Rumpf, M., Cremers, D.: Convex relaxation for grain segmentation at atomic scale. In: Fellner, D. (ed.) Vision, Modeling and Visualization. pp. 179–186. Eurographics Association (2010)
3. Bragg, W.L.: The determination of parameters in crystal structures by means of fourier series. In: Proceedings of the Royal Society of London A: Mathematical, Physical and Engineering Sciences. vol. 123, pp. 537–559. The Royal Society (1929)
4. Browning, N., Chisholm, M., Pennycook, S.: Atomic-resolution chemical analysis using a scanning transmission electron microscope. Nature 366(6451), 143–146 (1993)
5. Buades, A., Coll, B., Morel, J.M.: Image denoising methods. A new nonlocal principle. SIAM review 52(1), 113–147 (2010)
6. Burnham, K.P., Anderson, D.R.: Multimodel inference understanding aic and bic in model selection. Sociological methods & research 33(2), 261–304 (2004)
7. Cava, R., Ji, H., Fuccillo, M., Gibson, Q., Hor, Y.: Crystal structure and chemistry of topological insulators. Journal of Materials Chemistry C 1(19), 3176–3189 (2013)
8. Dabov, K., Foi, A., Katkovnik, V., Egiazarian, K.: Image Denoising by Sparse 3-D Transform-Domain Collaborative Filtering. Image Processing, IEEE Transactions on 16(8), 2080–2095 (2007)
9. De La Cuadra, P., Master, A., Sapp, C.: Efficient pitch detection techniques for interactive music. In: Proceedings of the 2001 International Computer Music Conference. pp. 403–406 (2001)
10. Elsey, M., Wirth, B.: Fast automated detection of crystal distortion and crystal defects in polycrystal images. Multiscale Modeling & Simulation 12(1), 1–24 (2014)
11. Hamerly, G., Elkan, C.: Learning the k in k-means. In: In Neural Information Processing Systems. p. 2003. MIT Press (2003)
12. Hanson, M.A., Roth, C.B., Jo, E., Griffith, M.T., Scott, F.L., Reinhart, G., Desale, H., Clemons, B., Cahalan, S.M., Schuerer, S.C., et al.: Crystal structure of a lipid g protein–coupled receptor. Science 335(6070), 851–855 (2012)
13. Kimoto, K., Asaka, T., Yu, X., Nagai, T., Matsui, Y., Ishizuka, K.: Local crystal structure analysis with several picometer precision using scanning transmission electron microscopy. Ultramicroscopy 110(7), 778–782 (2010)
14. Klug, A.: Image analysis and reconstruction in the electron microscopy of biological macromolecules. Chemica Scripta 14, 245–256 (1978–1979)
15. Klug, H.P., Alexander, L.E., et al.: X-ray diffraction procedures, vol. 2. Wiley New York (1954)
16. Mevenkamp, N., Binev, P., Dahmen, W., Voyles, P.M., Yankovich, A.B., Berkels, B.: Poisson noise removal from high-resolution stem images based on periodic block matching. Advanced Structural and Chemical Imaging 1(1), 1–19 (2015)
17. Pelleg, D., Moore, A.W.: X-means: Extending k-means with efficient estimation of the number of clusters. In: ICML. pp. 727–734 (2000)
18. Putnis, A.: An introduction to mineral sciences. Cambridge University Press (1992)

19. Sang, X., LeBeau, J.M.: Revolving scanning transmission electron microscopy: Correcting sample drift distortion without prior knowledge. Ultramicroscopy 138(0), 28 – 35 (2014), http://www.sciencedirect.com/science/article/pii/S0304399113003161
20. Wang, Z., Song, Y., Shi, H., Wang, Z., Chen, Z., Tian, H., Chen, G., Guo, J., Yang, H., Li, J.: Microstructure and ordering of iron vacancies in the superconductor system k y fe x se 2 as seen via transmission electron microscopy. Physical Review B 83(14), 140505 (2011)
21. Williams, D.B., Carter, C.B.: The transmission electron microscope. Springer (1996)
22. Zeng, Y.M., Wu, Z.Y., Liu, H.B., Zhou, L.: Modified amdf pitch detection algorithm. In: Machine Learning and Cybernetics, 2003 International Conference on. vol. 1, pp. 470–473. IEEE (2003)